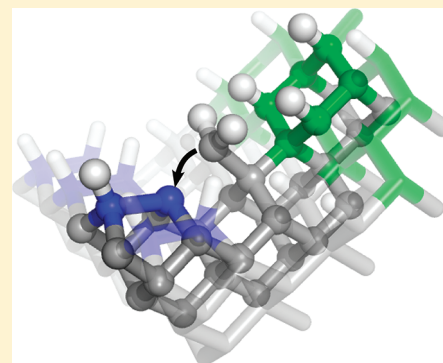


# CH<sub>2</sub> Group Migration between H-Terminated 2 × 1 Reconstructed {100} and {111} Surfaces of Diamond

James C. Richley,\* Jeremy N. Harvey,\* and Michael N. R. Ashfold\*

School of Chemistry, University of Bristol, Bristol BS8 1TS, United Kingdom

**ABSTRACT:** Successful growth of diamond by chemical vapor deposition requires that chemisorbed hydrocarbon species, most notably CH<sub>2</sub> groups, are able to migrate on the growing surface. Quantum mechanical and hybrid quantum mechanical/molecular mechanical (QM/MM) cluster models are here used to investigate the energetics of CH<sub>2</sub> migration on the C{111}:H surface and between C{100}:H 2 × 1 terraces separated by a region of C{111}:H surface. Many migration pathways of this type proceeding via structures involving 3-, 4-, and 5-membered rings are found to have relatively low barriers, so that migration should be relatively facile at typical diamond growth temperatures. In contrast, CH<sub>2</sub> migration via one particular C{111}:H/C{100}:H 2 × 1 step-edge geometry results in the formation of a very stable 6-membered ring intermediate. The energetics suggest that this process will be irreversible and should thus result in incorporation. This type of step-edge also occurs in the limiting case of two C{100}:H 2 × 1 terraces separated by a monolayer step, and migration of CH<sub>2</sub> species along the lower C{100}:H 2 × 1 terrace toward such step edges is predicted to favor incorporation. These findings offer a rationale for the deduced propensity for step-flow growth and the observation of stepped {100} terraces in CVD diamond samples.



## 1. INTRODUCTION

Growth of diamond films by chemical vapor deposition (CVD) from activated hydrocarbon/hydrogen gas mixtures is now a well-established technique.<sup>1,2</sup> The gas mixture is typically activated by either hot filament or microwave plasma enhanced techniques, and the diamond can be grown on a variety of substrates (typically maintained at temperatures,  $T_{\text{sub}} \approx 900\text{--}1200$  K). Activation results in H<sub>2</sub> dissociation and formation of H atoms. H atom addition and abstraction reactions with the input hydrocarbon yield a variety of gas phase hydrocarbon molecules and radicals. H atom abstraction reactions are also important in creating radical sites on the growing diamond surface, which is largely H-terminated under typical growth conditions. The most likely fate of any such radical site is retermination by another incident gas phase H atom. Occasionally, however, a carbon-containing radical will bond to one of these sites and, by a sequence of further reactions, be incorporated into (and thus extend) the diamond lattice.

The diamond {100} surface has been a longstanding topic for both theoretical and experimental studies due to the frequent showing of this low index surface in scanning electron microscopy images of as-grown CVD diamond samples and its simple cubic morphology. Steric constraints ensure that the fully H-terminated {100} surface has a 2 × 1 reconstructed structure with rows of surface carbon atoms paired as dimers.<sup>3–9</sup> Henceforth, we represent this surface as C{100}:H 2 × 1. The C{111}:H surface, in contrast, has a simple unreconstructed structure with a hydrogen atom terminating each surface carbon atom.<sup>10</sup> Figure 1 shows sections of two C{100}:H 2 × 1 terraces linked by a section

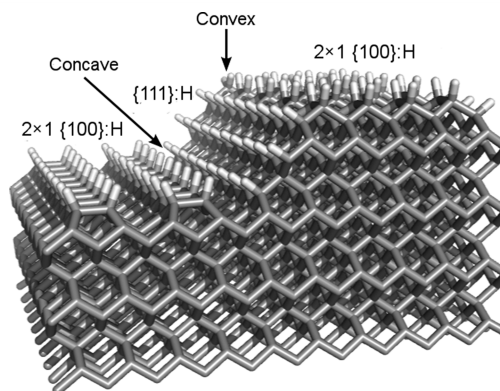


**Figure 1.** Overview of portions of two diamond C{100}:H 2 × 1 surfaces linked by a C{111}:H surface, illustrating the size of the slab used in the QM/MM simulations and what we term concave and convex step edges. Note that in this depiction the relative orientation of the C–C dimer bonds differ on the two C{100}:H 2 × 1 terraces, being, respectively, parallel on the upper terrace and perpendicular to the step edge on the lower terrace.

of C{111}:H surface, which serves as orientation for the migration studies that are the focus of the current work.

CH<sub>3</sub> radicals are now generally viewed as the primary growth species in most diamond CVD environments, and most theoretical studies of diamond CVD have focused on growth

Received: January 14, 2012

Revised: February 24, 2012

Published: March 19, 2012



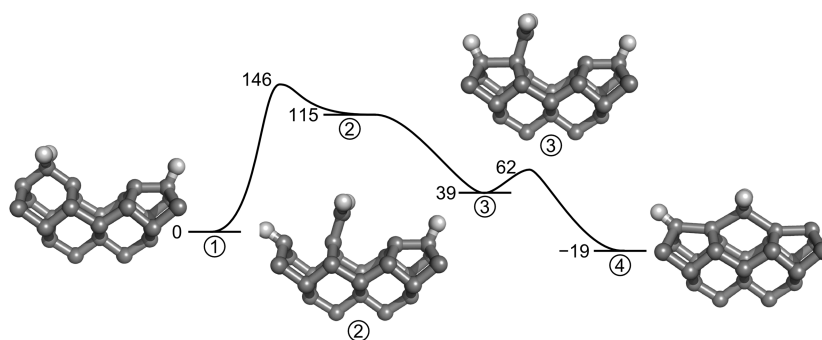


**Figure 2.** Summary of optimized initial (1) and selected intermediate (2, 3, and 4) structures returned by the QM/MM calculations for  $\text{CH}_2$  migration along a C–C dimer chain on the  $\text{C}\{100\}:\text{H } 2 \times 1$  surface. Relative energies (B3LYP, QM/MM, 6-311G(d,p):MM2), in  $\text{kJ mol}^{-1}$ , are quoted relative to that of structure 1 (after ref 13).

mechanisms initiated by  $\text{CH}_3$  addition to the  $\text{C}\{100\}:\text{H } 2 \times 1$  surface.<sup>1,2,11–14</sup> In order to be incorporated, a chemisorbed  $\text{CH}_3$  species must first be activated by H abstraction, forming a pendant  $\text{CH}_2$  group. Incorporating this into the bulk crystal structure requires subsequent surface rearrangement (either ring-opening/closing, in the case that the  $\text{CH}_2$  is incorporated into what was previously a C–C dimer bond,<sup>1,2,5–7</sup> or trough bridging, in the case that the insertion is between two dimer bonds<sup>8</sup>) and further reaction with a gas phase H atom.  $\text{CH}_3$  radical addition and subsequent growth on the  $\{111\}:\text{H}$  surface has also been investigated previously.<sup>15–17</sup> The addition of single carbon species to the  $\{100\}$  and  $\{111\}$  surfaces as outlined above would be expected to occur at random sites. Such additions cannot explain the locally smooth surface morphologies that are observed experimentally, unless the  $\text{CH}_2$  groups are able to migrate, postincorporation. The energetics of such migrations have been investigated theoretically on both the H-terminated  $\text{C}\{100\}:\text{H } 2 \times 1$ <sup>5,12,18–20</sup> and  $\text{C}\{111\}:\text{H}$ <sup>21</sup> surfaces. Migration in both cases requires the presence of a surface radical site adjacent to the pendant  $\text{CH}_2$  as illustrated in Figure 2. The  $\text{CH}_2$  group and the surface radical react to form a bridging ring structure. Subsequent ring-opening results in the  $\text{CH}_2$  group migrating along the surface by one carbon atom, or reversion to the original structure.

The migration and incorporation of  $\text{CH}_2$  groups at step-edges has been suggested<sup>18</sup> as a possible explanation for the frequently observed stepped texture of the  $\{100\}$  surfaces of CVD diamond films and of diamonds subjected to hydrogen plasma etching, but the energetics of migration at the step-edge between two intersecting crystal planes has received little attention thus far. Yet the facility, or otherwise, of such processes will be important in determining the morphology of CVD films, as highlighted in recent kinetic Monte Carlo modeling studies of diamond growth.<sup>22,23</sup> The present work employs quantum mechanical (QM) and hybrid quantum mechanical/molecular mechanical (QM/MM) cluster models to investigate (i) migration pathways of a  $\text{CH}_2$  group on the  $\text{C}\{111\}:\text{H}$  surface further, (ii) possible migration routes between the  $\text{C}\{100\}:\text{H } 2 \times 1$  and  $\text{C}\{111\}:\text{H}$  surfaces, and (iii) incorporation at step-edges between such surfaces, with a view to providing a rationale for the deduced propensity for step-flow growth in diamond CVD,<sup>24–26</sup> and the formation of  $\{100\}$  terraces.

## 2. COMPUTATIONAL DETAILS

Most of the calculations described in this work are hybrid QM/MM calculations, performed using the QoMMMa program,<sup>27,28</sup>

wherein a QM region (calculated using Jaguar 5.0<sup>29</sup>) is embedded within a much larger MM region that is modeled with TINKER.<sup>30</sup> As before,<sup>13</sup> the QM/MM model is based on a  $5 \times 9 \times 4$  slab (defined in terms of numbers of C–C dimer bonds), with an initial geometry defined by the bulk diamond lattice points. The positions of the peripheral atoms (with nonchemical stoichiometry) are held frozen during the calculations. The energy of the QM region was described using the B3LYP density functional with the 6-31G(d) basis set, while the MM region was treated with the MM2 protocol. Coupling between the two regions was described using nonbonded Lennard-Jones terms as well as hydrogen link atoms to saturate valences in the QM region. More accurate single point QM/MM energies were then calculated for the optimized geometries by recomputing the energy of the QM region, still with the B3LYP density functional, but with the larger 6-311G(d,p) basis set. This output was added to the MM energy and the QM/MM nonbonded interaction energy to yield the final QM/MM energies, which are reported here without correction for zero-point energy.

The initial and final species in each of the migration pathways investigated include a pendant  $\text{CH}_2$  group adjacent to a surface radical site, and thus involve two unpaired electrons. The intermediate ring-closed structure, in contrast, will have a closed-shell electronic configuration. The energies for the triplet and open-shell singlet electronic states of the initial and final species were both derived using an unrestricted DFT ansatz, while a restricted closed-shell DFT ansatz was used for the intermediate ring closed structure. Energies of calculated open-shell singlet states were found to lie within  $10 \text{ kJ mol}^{-1}$  of the corresponding triplet state for most of the structures studied.

As before,<sup>13,31</sup> approximate transition states (TSs) were identified by calculating the energy of the system at a series of values along a chosen reaction coordinate using a harmonic constraint to hold the system close to the required value; the structure is allowed to relax in all other degrees of freedom. For the migration pathways of current interest, the chosen reaction coordinate  $R$  was defined by  $(R_1 - R_2)$  where  $R_1$  and  $R_2$  are, respectively, the separation of the pendant  $\text{CH}_2$  group from the surface carbon to which it is attached and the distance between this same  $\text{CH}_2$  group and the adjacent surface radical site as illustrated in Figure 3. The energy of the TS was taken as the maximum energy along a curve produced by plotting the single point QM/MM energy against  $R$ . Unless stated otherwise, the single point QM/MM energies reported for the intermediate, final, and transition states are all defined (in  $\text{kJ mol}^{-1}$ ) relative

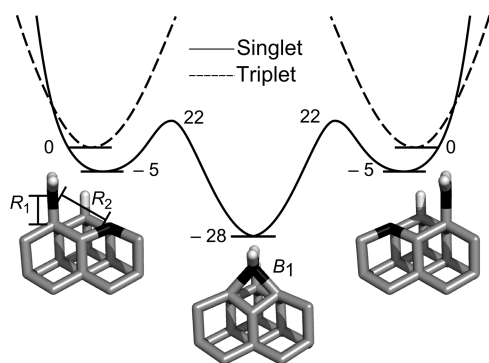


**Figure 3.** Calculated minimum energy profile and optimized geometries of initial, intermediate, and final QM structures returned by the QM/MM calculations for CH<sub>2</sub> migration on the C{111}:H surface. Also shown are the respective energies (B3LYP QM/MM 6-311G(d,p):MM2 basis set) in kJ mol<sup>-1</sup>, defined relative to that of the initial structure in its triplet electronic state. The R<sub>1</sub> and R<sub>2</sub> bond lengths used to define the reaction coordinate R are shown on the starting structure, and the B<sub>1</sub> bond length discussed in the text is indicated on the intermediate structure.

to that of the triplet state of the initial species, which we define as  $E = 0$ .

For one system, QM-only B3LYP calculations were carried out on a smaller cluster model, using the 6-31G(d) basis set and the Gaussian03 package.<sup>32</sup> In this case, the structure of the minimum energy crossing point between singlet and triplet surfaces was optimized using our own code.<sup>33</sup> Briefly, this code creates singlet and triplet input files for Gaussian at the current structure, runs single-point calculations, and extracts the energy and gradient on both surfaces, combining them to yield an effective gradient, which is then used for optimization.

### 3. RESULTS AND DISCUSSION

CH<sub>2</sub> migration on an H-terminated diamond surface requires the presence of an adjacent surface radical site.<sup>11,13,18–21</sup> The sequence of ring closing and opening reactions then results in the CH<sub>2</sub> group migrating along the surface by one carbon atom, or it is a null event. In the present calculations, the necessary adjacent radical site is assumed already to be present, and attention is focused on the ring closing and opening processes, which permit migration. Here, we first describe new calculations for CH<sub>2</sub> migration on the C{111}:H surface, then explore various possible migration routes between the C{100}:H 2 × 1 and C{111}:H surfaces. The focus of the present study, wherein a single C<sub>1</sub>H<sub>x</sub> ( $x = 3, 2$ ) species adsorbs, is activated, and then migrates, is likely to be most applicable to growth of high quality diamond from dilute hydrocarbon/H<sub>2</sub> gas mixtures. Additional growth species and multiple (and cooperative) adsorption and migration events are likely to become increasingly important when describing growth from gas mixtures containing higher hydrocarbon mole fractions and at higher gas (and substrate) temperatures, such as used for depositing (ultra)nanocrystalline diamond.<sup>34</sup>

**3.1. Migration on the C{111}:H Surface.** Migration of CH<sub>2</sub> groups on the C{111}:H surface has been investigated previously by Larsson et al. using a cluster approach and second order Møller–Plesset perturbation theory, as well as additional DFT calculations using a periodic slab model.<sup>21</sup> The energies established in the present work are in good qualitative accord with the results of that earlier study. We report our own calculations here for completeness and to allow comparison

with the results obtained for the novel migration steps discussed later. We also use this particular case to consider carefully the role of the triplet and singlet pathways along the reaction coordinate.

Figure 3 shows optimized initial, intermediate, and final structures of the QM region returned by the present QM/MM calculations for CH<sub>2</sub> migration on the C{111}:H surface with the energies (B3LYP, QM/MM, and 6-311G(d,p) basis set) quoted relative to that of the starting structure. Migration proceeds via a 4-membered ring intermediate that lies 28 kJ mol<sup>-1</sup> below the initial ring-open state. An approximate TS for the ring-closing reaction was located at  $E = +22$  kJ mol<sup>-1</sup> (i.e., somewhat lower than the +52 kJ mol<sup>-1</sup> returned in the earlier study<sup>21</sup>). Thus, the barrier to CH<sub>2</sub> migration on the C{111}:H surface is appreciably lower than that for CH<sub>2</sub> migration along the dimer chains and rows on the C{100}:H 2 × 1 surface (calculated at  $E = +145$  and +105 kJ mol<sup>-1</sup>, respectively<sup>13</sup>). Under standard CVD conditions, therefore, CH<sub>2</sub> migration on the C{111}:H surface is likely to be a facile process limited, primarily, by the availability of adjacent radical sites.

It is important to note that the initial and final biradical species in this migration process have close-lying spin singlet and triplet states, whereas the 4-membered ring intermediate is a closed-shell singlet. Hence, the migration process potentially involves two changes of spin state. We have suggested previously<sup>13</sup> that spin-state changes should not be rate limiting when required in reactions at the diamond surface. Separate B3LYP/6-31G(d) calculations have now been performed on the cluster corresponding to the QM region used in the QM/MM study (including its capping H link atoms) to explore in more detail the spin state changes involved in this reaction. These calculations lead to optimized structures and relative energies that are very similar to those obtained with the QM/MM approach. The triplet diradical lies 10 kJ mol<sup>-1</sup> higher in energy than the corresponding open-shell singlet, and the 4-membered ring intermediate lies 111 kJ mol<sup>-1</sup> lower than the singlet diradical. The minimum energy crossing point (MECP) between the triplet and singlet potential energy surfaces (PESs) in the vicinity of the triplet diradical minimum was also located and found to lie ~2 kJ mol<sup>-1</sup> above the triplet minimum. This means that the seam of intersection between singlet and triplet surfaces will be crossed repeatedly at diamond surface temperatures ( $T_{\text{sub}} \approx 900$ –1200 K), and even the small spin–orbit and spin–spin coupling matrix elements<sup>35</sup> should suffice to enable rapid interconversion between singlet and triplet states.<sup>36</sup> Reactive transformations may thus be assumed to proceed on whichever PES has the lower barrier, i.e., under Curtin–Hammett conditions.<sup>37</sup> We have assumed that such rapid equilibration is operative in all other cases below and do not discuss spin-state changes further.

We note that the small QM model predicts a much greater stability for the 4-membered ring intermediate species relative to the initial triplet diradical ( $\Delta E = -111$  kJ mol<sup>-1</sup> at the B3LYP/6-31G(d) level) than the QM/MM calculations ( $-28$  kJ mol<sup>-1</sup>, B3LYP/6-311G(d) single point energies;  $-40$  kJ mol<sup>-1</sup> with 6-31G(d)). The QM system can tolerate greater distortions than the QM/MM model, and this difference leads to greater strain in the 4-membered ring in the latter calculations. This is reflected by an unfavorable MM contribution to the energy of ring formation in the QM/MM calculations (+22 kJ mol<sup>-1</sup>) and by the longer predicted C–C bond lengths. For example, the QM/MM model returns a value

of 1.653 Å for the  $B_1$  bond length in Figure 3, whereas the corresponding QM model calculation gives 1.610 Å.

**3.2. Step-Edge Migration.** As Figure 1 showed, two types of step-edge can be envisaged at the intersection of  $C\{111\}:H$  and  $C\{100\}:H$   $2 \times 1$  surfaces, which we term convex and concave. These subdivide further, depending on the orientation (parallel or perpendicular) of the dimer bonds on the  $C\{100\}:H$   $2 \times 1$  surface relative to the step-edge. Thus, we need to consider two possible pathways for migration on the convex step-edge and three different pathways for migration on the concave step-edge (due to two possible initial locations of the  $CH_2$  group in the case that the dimer bonds run parallel to the step-edge), each of which requires use of a slight variation of the base QM/MM model. In what follows, we describe motion of a  $CH_2$  group over these step-edges in one general direction: starting from a top  $C\{100\}:H$   $2 \times 1$  surface, over a convex step-edge and onto a  $C\{111\}:H$  surface, then from the latter over a concave step-edge, onto a lower  $C\{100\}:H$   $2 \times 1$  surface. Most of the migration processes are roughly thermoneutral, however, so migration of a  $CH_2$  group in the opposite direction is generally also possible.

**3.2.1. Convex Step-Edge.** We first consider a  $CH_2$  group migrating from the  $C\{100\}:H$   $2 \times 1$  surface to the  $C\{111\}:H$  diamond surface when the dimer bonds on the former are aligned perpendicular to the convex step edge, as illustrated in Figure 4a. Migration proceeds via a 4-membered cyclic

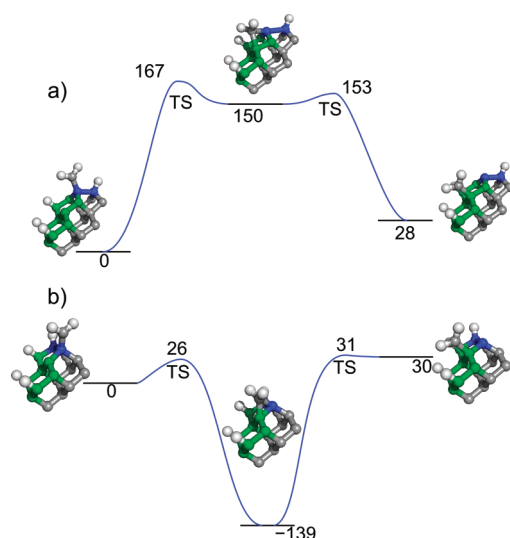


**Figure 4.** Calculated minimum energy profiles for  $CH_2$  migration from the  $C\{100\}:H$   $2 \times 1$  surface to the  $C\{111\}:H$  surface via a convex step-edge with the dimer bonds on the former aligned (a) perpendicular and (b) parallel to the step-edge, together with depictions of the optimized initial, intermediate, and final QM structures returned by the QM/MM calculations. Carbon atoms on the  $C\{100\}:H$   $2 \times 1$  surface are highlighted in blue, while those on the  $C\{111\}:H$  surface are green. The reported energies are from B3LYP/6-311G(d,p):MM2 calculations, defined relative to the initial structure, in  $\text{kJ mol}^{-1}$ .

intermediate, lying at  $E = +150 \text{ kJ mol}^{-1}$ . The high energy of this ring-closed intermediate is likely due to the induced strain distorting the dimer bond on the upper  $\{100\}:H$   $2 \times 1$  terrace away from its ideal position, as can be observed in the QM regions shown in Figure 4a. The final diradical structure, with the  $CH_2$  group now located on the  $C\{111\}:H$  diamond surface, is calculated to lie  $28 \text{ kJ mol}^{-1}$  above the starting structure.

Approximate TSs for the ring closing and opening steps have also been located, at  $E = +167 \text{ kJ mol}^{-1}$  and  $+153 \text{ kJ mol}^{-1}$ , respectively, as shown in Figure 4a. These barrier energies are similar to those described previously for migration on the  $C\{100\}:H$   $2 \times 1$  surface.<sup>13</sup> In that work, it was argued that such barriers would lead to migration with rate constants of  $\sim 10^8 \text{ s}^{-1}$ , at typical diamond growth temperatures, and similar rate constants should be expected for the processes described here.

As Figure 4b shows,  $CH_2$  migration when the dimer bonds on the  $C\{100\}:H$   $2 \times 1$  surface are parallel to the convex step-edge involves passage via a 3-membered ring structure, lying  $139 \text{ kJ mol}^{-1}$  below that of the initial structure, to yield a final diradical lying at  $E = +30 \text{ kJ mol}^{-1}$ . The predicted exothermicity of the ring closing reaction is smaller than that typically associated with C–C bond formation, again reflecting the strained nature of the intermediate ring structure. Approximate TSs for the ring-closing and ring-opening steps in this case are found at  $E = +26$  and  $+31 \text{ kJ mol}^{-1}$ .

The rate limiting step in the former migration pathway (Figure 4a) will be the formation of the strained 4-membered ring, whereas, in the latter, it is likely to be the ring-opening step. The relative rates of the two possible migrations will depend sensitively upon the efficiency (or otherwise) with which the exothermicity of the ring-closing step in the latter is dissipated into the bulk. In the least favorable scenario, the 3-membered ring intermediate will be fully thermally equilibrated with the bulk, and the barrier to forming the migrated diradical structure will be comparable to that in Figure 4a. Both endoergicities are larger than those calculated for  $CH_2$  migration on the  $C\{100\}:H$   $2 \times 1$  surface (and much larger than for migration on the  $C\{111\}:H$  surface), but neither is expected to be prohibitive at the substrate temperatures prevailing in most diamond CVD environments.

**3.2.2. Concave Step-Edge.** As at the convex step-edge, we identify different migration routes depending on the relative alignment of the dimer bonds on the  $C\{100\}:H$   $2 \times 1$  surface with respect to a concave step-edge. One migration pathway from the  $C\{111\}:H$  to the  $C\{100\}:H$   $2 \times 1$  surface exists when the dimer bonds on the latter are perpendicular to the step-edge. This we, henceforth, label as P1. Two further migration pathways can be identified for the case that the dimer bonds are parallel to the step-edge. These are distinguished by the initial location of the migrating  $CH_2$  group on the  $C\{111\}:H$  surface, which can either be facing a trough between dimers on the  $C\{100\}:H$   $2 \times 1$  surface or be directed toward the middle of a dimer bond. These latter two pathways we label P2 and P3, respectively.

Optimized geometries and energies have been calculated for the initial structures (i.e.,  $CH_2$  group on the  $C\{111\}:H$  surface), intermediate ring-closed structures, and the final postmigration structures (i.e.  $CH_2$  on the  $C\{100\}:H$   $2 \times 1$  surface) for each of pathways P1–P3. All three pathways are found to be mildly exothermic, with the final diradical species lying at  $E = -99$  (P1),  $-34$  (P2), and  $-60$  (P3)  $\text{kJ mol}^{-1}$ , respectively. Five-membered ring intermediates were identified for pathways P2 and P3, with relative energies of  $E = -116$  and  $E = -165 \text{ kJ mol}^{-1}$  defined relative to their respective initial diradical structures. Pathway P1 proceeds via a more stable 6-membered ring intermediate, with an associated energy-well  $E = -356 \text{ kJ mol}^{-1}$ . These calculated energy profiles for pathways P1–P3 are included in Figure 5. We were unable to locate approximate TSs for any of the ring-closing and ring-opening steps, and we therefore assume that these processes are barrierless (or nearly

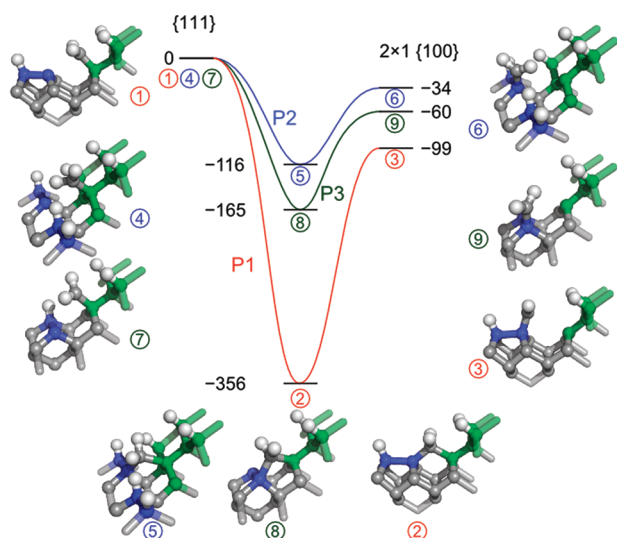


**Figure 5.** Calculated minimum energy profiles for  $\text{CH}_2$  migration from the  $\text{C}\{111\}:\text{H}$  surface to the  $\text{C}\{100\}:\text{H}$   $2 \times 1$  surface via a concave step-edge. P1: dimer bonds on the latter are perpendicular to the step-edge (Structures 1–3). P2 and P3: dimer bonds are parallel to the step-edge (Structures 4–6 and 7–9 for pathways P2 and P3, respectively). Carbon atoms on the  $\text{C}\{100\}:\text{H}$   $2 \times 1$  surface are highlighted in blue, while those on the  $\text{C}\{111\}:\text{H}$  surface are green. The quoted energies ( $\text{kJ mol}^{-1}$ ) are from B3LYP/6-311G(d,p):MM2 calculations, defined relative to the initial structure.

so). Indeed, these migration pathways are each sufficiently similar to the case where the dimer rows are parallel to the convex step-edge (Figure 4b), that it is reasonable to anticipate negligible barrier to forming the intermediate ring-closed structures.

Given these energy profiles, we conclude that migration of a  $\text{CH}_2$  group from the  $\text{C}\{111\}:\text{H}$  to the  $\text{C}\{100\}:\text{H}$   $2 \times 1$  surface, and vice versa, via pathways P2 and P3 will be rather facile under standard CVD conditions. The deep energy minimum calculated for pathway P1, in contrast, implies that once a  $\text{CH}_2$  group forms the 6-membered ring structure, it is likely to be locked in place (i.e. incorporated into the diamond lattice at the step edge), reinforcing an earlier conclusion of Frenklach et

al.,<sup>20</sup> based on less accurate semiempirical electronic structure calculations.

**3.2.3. Migration over a Single-Layer Step-Edge.** Scanning tunnelling microscopy<sup>7</sup> images of macroscopic crystal facets present on  $\text{C}\{100\}:\text{H}$   $2 \times 1$  surfaces of diamond reveal stepped terraces when viewed on the atomic scale. Many of these terraces are separated by just one intermediate layer of carbon atoms, leading to two types of step-edge, often labeled  $S_A$  and  $S_B$ .<sup>23,38</sup> These are distinguished by the orientation of the C–C dimer bonds on the upper  $\{100\}$  terrace relative to the step-edge, normal in the case of  $S_A$  and parallel for  $S_B$ . Migration of a  $\text{CH}_2$  group down or up an  $S_A$  step-edge is expected to occur with energetics similar to those shown in Figures 4a and 6 and so, as was argued above, should occur with comparable ease to migration along a  $\text{C}\{100\}:\text{H}$   $2 \times 1$  terrace. Migration toward an  $S_B$  step-edge could lead to the formation of a 6-membered intermediate structure capable of promoting step-flow growth at the step-edge (recall Figure 5, P1) and is thus of more interest. Accordingly, we have carried out additional calculations on  $\text{CH}_2$  radical migration between two  $\text{C}\{100\}:\text{H}$   $2 \times 1$  terraces separated by this single-layer step-edge.

Figure 6 shows the QM/MM calculated minimum energy profile for a  $\text{CH}_2$  group migrating down a  $S_B$  step-edge. The zero of energy is here taken as the fully H-terminated structure 1. The initial steps  $1 \rightarrow 2 \rightarrow 3$  are reminiscent of those shown in Figure 4b for the migration of a  $\text{CH}_2$  group over the convex step-edge. The formation of the ring-closed intermediate 2 is exothermic,  $\Delta E = -148 \text{ kJ mol}^{-1}$ , and proceeds via a TS lying  $\sim 10\text{--}20 \text{ kJ mol}^{-1}$  above the initial structure 1. The ring-opening step  $2 \rightarrow 3$ , which has the effect of moving the  $\text{CH}_2$  down the single-layer step-edge, is more endoergic ( $\Delta E = +250 \text{ kJ mol}^{-1}$  vs  $+169 \text{ kJ mol}^{-1}$ ) than the corresponding step in Figure 4b. This presumably reflects the different level of strain in the two 3-membered ring species, which are attached to the diamond bulk in different ways. There may also be increased steric hindrance from the adjacent surface H atom in species 3 in Figure 6. An energy scan suggests that there is no potential energy barrier to the ring-opening process. After roughly thermoneutral hydrogen atom transfer steps leading from 3, through 4 to 5, the second stage of the migration process can

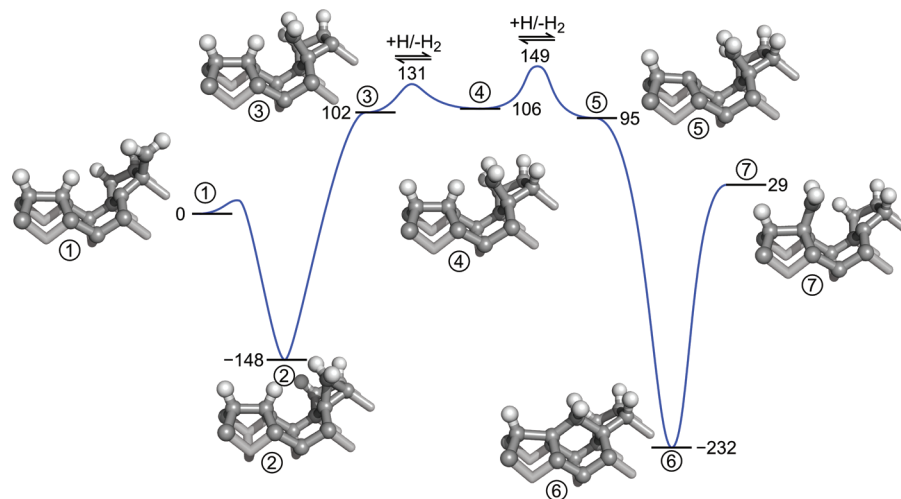


**Figure 6.** Calculated minimum energy profiles for  $\text{CH}_2$  migration from between two  $\text{C}\{100\}:\text{H}$   $2 \times 1$  surfaces separated by a single-layer step, with the dimer bonds on the upper surface aligned parallel to the step-edge (i.e. a type  $S_B$  step-edge). The calculated energies (in  $\text{kJ mol}^{-1}$ ) are all defined relative to that of structure 1.

occur. This process resembles pathway P1 on the concave step-edge (Figure 5, P1), and the calculated energetics are rather similar. Formation of the ring closed intermediate 6 is highly exothermic ( $\Delta E = -327 \text{ kJ mol}^{-1}$  (relative to the structure 5)) and the  $\text{CH}_2$  group is more stable on the  $\text{C}\{100\}:\text{H } 2 \times 1$  surface (structure 7) than in between the two terraces (structure 5). The energy for the ring-closing step leading from 5 to 6 was also calculated for the same type of step edge site in ref 23 but using a reactive molecular mechanics empirical PES. The calculated exothermicity of 2.49 eV ( $\Delta E = -240 \text{ kJ mol}^{-1}$ ) is comparable, albeit lower than the  $\Delta E = -327 \text{ kJ mol}^{-1}$  found here using DFT QM/MM.

Unlike the processes described above, the net activation energy for migration of a  $\text{CH}_2$  group between the two  $\text{C}\{100\}:\text{H } 2 \times 1$  terraces of a single-layer  $\text{S}_B$  step-edge is quite high, at  $+297 \text{ kJ mol}^{-1}$  starting from the upper terrace, or  $+381 \text{ kJ mol}^{-1}$  starting from the lower terrace. Such migrations are thus considered unlikely (though migrations across the  $\text{S}_A$  step-edge should be feasible). The most probable fate for a  $\text{CH}_2$  species migrating on the lower terrace at typical growth temperatures and arriving at the base of the step-edge will be incorporation (i.e.,  $7 \rightarrow 6$ , constituting step-flow growth on the atomic scale). A  $\text{CH}_2$  group approaching the step-edge on the upper terrace (i.e.  $1 \rightarrow 2$ ), in contrast, will most likely be able to escape from the ring-closed structure 2 and revert to migrating on the upper terrace. Recalling Figures 4 and 5, it is tempting to suggest that this blockade is a particular feature of the single-layer step-edge and the greater steric impediment to  $\text{CH}_2$  migration that it presents (relative to the case of larger interterrace steps).

#### 4. CONCLUSIONS

The mechanisms and energetics of migration of a  $\text{CH}_2$  group on the  $\text{C}\{111\}:\text{H}$  surface and between  $\text{C}\{100\}:\text{H } 2 \times 1$  terraces separated by a region of  $\text{C}\{111\}:\text{H}$  surface have been explored using QM and QM/MM cluster models. In most cases, the barrier heights encountered in migration pathways proceeding via 3-, 4-, or 5-membered ring closed structures are not much greater than that calculated for migration along a dimer chain on the  $\text{C}\{100\}:\text{H } 2 \times 1$  surface. Such migrations are thus deduced to be feasible at typical diamond growth temperatures, provided the required diradical species can be formed through hydrogen abstraction steps with gas phase H atoms. The energy profiles of reaction sequences that involve a 6-membered intermediate at the step-edge exhibit much deeper potential wells and are more likely to result in incorporation. One such example arises when two  $\text{C}\{100\}:\text{H } 2 \times 1$  terraces are separated by a single layer of carbon atoms: migration along the lower  $\text{C}\{100\}:\text{H } 2 \times 1$  terrace leads to a stable 6-membered ring species upon encountering a step-edge with the  $\text{S}_B$  configuration. Migration from an upper to a lower terrace at an  $\text{S}_B$  step-edge thus appears to be an exception to the rule whereby migration across step-edges is relatively facile.

#### AUTHOR INFORMATION

##### Corresponding Author

\*Tel: +44 117 9288312 (M.N.R.A.); +44 117 9546991 (J.N.H.). Fax: +44 117 9250612. E-mail: Jeremy.Harvey@bristol.ac.uk (J.N.H.); mike.ashfold@bris.ac.uk (M.N.R.A.).

##### Notes

The authors declare no competing financial interest.

#### ACKNOWLEDGMENTS

We are grateful to EPSRC for the award of a research grant and studentship (to J.C.R.) and to Element Six Ltd. for financial support.

#### REFERENCES

- (1) Goodwin, D. G.; Butler, J. E. In *Handbook of Industrial Diamonds and Diamond Films*; Prelas, M. A., Popovici, G., Bigelow, L. G., Eds.; Marcel Dekker: New York, 1998; pp 527–581.
- (2) Butler, J. E.; Mankelevich, Y. A.; Cheesman, A.; Ma, J.; Ashfold, M. N. R. *J. Phys.: Condens. Matter* **2009**, *21*, 364201.
- (3) Tsuno, T.; Tomikawa, T.; Shikata, S.; Imai, T.; Fujimori, N. *Appl. Phys. Lett.* **1994**, *64*, 572.
- (4) Thoms, B. D.; Butler, J. E. *Surf. Sci.* **1995**, *328*, 291.
- (5) Nützenadel, C.; Küttel, O. M.; Diederich, L.; Maillard-Schaller, E.; Gröning, O.; Schlapbach, L. *Surf. Sci.* **1996**, *396*, L111.
- (6) Kawarada, H.; Sasaki, H.; Sato, A. *Phys. Rev. B* **1995**, *52*, 11351.
- (7) Stallcup, R. E. II; Perez, J. M. *Phys. Rev. Lett.* **2001**, *86*, 3368.
- (8) Bobrov, K.; Mayne, A.; Comtet, G.; Dujardin, G.; Hellner, L.; Hoffman, A. *Phys. Rev. B* **2003**, *68*, 195416.
- (9) Nimmrich, M.; Kittelmann, M.; Rahe, P.; Mayne, A. J.; Dujardin, G.; von Schmidsfeld, A.; Reichling, M.; Harheit, W.; Kühnle, A. *Phys. Rev. B* **2010**, *81*, 201403(R).
- (10) Pate, B. B. *Surf. Sci.* **1986**, *165*, 83.
- (11) Skokov, S.; Weiner, B.; Frenklach, M. *J. Phys. Chem.* **1994**, *98*, 7073.
- (12) Tamura, H.; Zhou, H.; Hirano, Y.; Takami, S.; Kubo, M.; Belosludov, R. V.; Miyamoto, A.; Imamura, A.; Gamo, M. N.; Ando, T. *Phys. Rev. B* **2000**, *62*, 16995.
- (13) Cheesman, A.; Harvey, J. N.; Ashfold, M. N. R. *J. Phys. Chem. A* **2008**, *112*, 11436.
- (14) Garrison, B. J.; Dawnkaski, E. J.; Srivastava, D.; Brenner, D. W. *Science* **1992**, *255*, 835.
- (15) Tsuda, M.; Nakajima, M.; Oikawa, S. *J. Am. Chem. Soc.* **1986**, *108*, 5780.
- (16) Battaile, C. C.; Srolovitz, D. J.; Butler, J. E. *Diamond Relat. Mater.* **1997**, *6*, 1198.
- (17) Butler, J. E.; Oleynik, I. *Philos. Trans. R. Soc., A* **2008**, *366*, 295.
- (18) Frenklach, M.; Skokov, S. *J. Phys. Chem. B* **1997**, *101*, 3025.
- (19) Skokov, S.; Weiner, B.; Frenklach, M.; Frauenheim, T.; Sternberg, M. *Phys. Rev. B* **1995**, *52*, 5426.
- (20) Frenklach, M.; Skokov, S.; Weiner, B. *Nature* **1994**, *372*, 535.
- (21) Larsson, K.; Carlsson, J. O. *Phys. Rev. B* **1999**, *59*, 8315.
- (22) May, P. W.; Harvey, J. N.; Allan, N. L.; Richley, J. C.; Mankelevich, Y. A. In *Diamond Electronics and Bioelectronics—Fundamentals to Applications III*; Bergonzo, P., Butler, J. E., Jackman, R. B., Loh, K. P., Nesladek, M., Eds.; Mater. Res. Soc. Symp. Proc., Vol. 1203; Materials Research Society: Warrendale, PA, 2010; paper J16-02.
- (23) Eckert, M.; Neyts, E.; Bogaerts, A. *Cryst. Growth Des.* **2010**, *10*, 4123.
- (24) Van Enckevort, W. J. P.; Janssen, G.; Vollenberg, W.; Schermer, J. J.; Giling, L. J.; Seal, M. *Diamond Relat. Mater.* **1993**, *2*, 997.
- (25) Larsson, K. *Phys. Rev. B* **1997**, *56*, 15452.
- (26) Netto, A.; Frenklach, M. *Diamond Relat. Mater.* **2005**, *14*, 1630.
- (27) Harvey, J. N. *Faraday Discuss.* **2004**, *127*, 165.
- (28) Tsipis, A. C.; Orpen, A. G.; Harvey, J. N. *Dalton Trans.* **2005**, 2849.
- (29) *Jaguar: Rapid ab Initio Electronic Structure Package*; Schrödinger Inc.: Portland, OR, 2000.
- (30) Ponder, J. W. *TINKER: Software Tools for Molecular Design, v4.0*; Washington University: Saint Louis, MO, 2003.
- (31) Richley, J. C.; Harvey, J. N.; Ashfold, M. N. R. *J. Phys. Chem. A* **2009**, *113*, 11416.
- (32) Frisch, M. J.; Trucks, G. W.; Schlegel, H. B.; Scuseria, G. E.; Robb, M. A.; Cheeseman, J. R.; Montgomery, J. A., Jr.; Vreven, T.; Kudin, K. N.; Burant, J. C.; Millam, J. M.; Iyengar, S. S.; Tomasi, J.; Barone, V.; Mennucci, B.; Cossi, M.; Scalmani, G.; Rega, N.;

Petersson, G. A.; Nakatsuji, H.; Hada, M.; Ehara, M.; Toyota, K.; Fukuda, R.; Hasegawa, J.; Ishida, M.; Nakajima, T.; Honda, Y.; Kitao, O.; Nakai, H.; Klene, M.; Li, X.; Knox, J. E.; Hratchian, H. P.; Cross, J. B.; Bakken, V.; Adamo, C.; Jaramillo, J.; Gomperts, R.; Stratmann, R. E.; Yazyev, O.; Austin, A. J.; Cammi, R.; Pomelli, C.; Ochterski, J. W.; Ayala, P. Y.; Morokuma, K.; Voth, G. A.; Salvador, P.; Dannenberg, J. J.; Zakrzewski, V. G.; Dapprich, S.; Daniels, A. D.; Strain, M. C.; Farkas, O.; Malick, D. K.; Rabuck, A. D.; Raghavachari, K.; Foresman, J. B.; Ortiz, J. V.; Cui, Q.; Baboul, A. G.; Clifford, S.; Cioslowski, J.; Stefanov, B. B.; Liu, G.; Liashenko, A.; Piskorz, P.; Komaromi, I.; Martin, R. L.; Fox, D. J.; Keith, T.; Al-Laham, M. A.; Peng, C. Y.; Nanayakkara, A.; Challacombe, M.; Gill, P. M. W.; Johnson, B.; Chen, W.; Wong, M. W.; Gonzalez, C.; Pople, J. A. *Gaussian 03*, revision B.04; Gaussian, Inc.: Wallingford, CT, 2003.

(33) Harvey, J. N.; Aschi, M. *Phys. Chem. Chem. Phys.* **1999**, *1*, 5555.

(34) May, P. W.; Harvey, J. N.; Allan, N. L.; Richley, J. C.; Mankelevich, Y. A. *J. Appl. Phys.* **2010**, *108*, 014905.

(35) Michl, J. *J. Am. Chem. Soc.* **1996**, *118*, 3568.

(36) Harvey, J. N. *Phys. Chem. Chem. Phys.* **2007**, *9*, 331.

(37) Seeman, J. I. *Chem. Rev.* **1983**, *83*, 84.

(38) Chadi, D. J. *Phys. Rev. Lett.* **1987**, *59*, 1691.